JOURNAL OF COMPUTATIONAL PHYSICS **129,** 364–382 (1996)
ARTICLE NO. 0256

A Sequel to AUSM: AUSM$^+$

Meng-Sing Liou

Internal Fluid Mechanics Division, NASA Lewis Research Center, Cleveland, Ohio 44135
E-mail: fsmsl@yinyan.lerc.nasa.gov

Received March 6, 1995; revised July 23, 1996

While enjoying demonstrated improvement in accuracy, efficiency, and robustness over existing schemes, the advection upstream splitting method (AUSM) has been found to have deficiencies in some cases. This paper describes recent progress toward improving the AUSM. We show that the improved scheme, termed AUSM$^+$, features the following properties: (1) exact resolution of 1D contact and shock discontinuities, (2) positivity preserving of scalar quantity such as the density, (3) free of "carbuncle phenomenon," (4) free of oscillations at the slowly moving shock, (5) algorithmic simplicity, and (6) easy entension to treat other hyperbolic systems. In this paper, we lay out a general construction for the AUSM$^+$ scheme and prove its heretofore unreported mathematical properties. Especially a CFL-like condition for positivity-preserving property is derived. This positivity-preserving proves to be tightly related to the capability of calculating strong rarefaction and near vacuum flows. Finally, results of numerical tests on many problems are given to confirm the capability and improvements on a variety of problems including those failed by other well-known schemes.

1. INTRODUCTION

Seeking an *accurate* numerical scheme for capturing shock and contact discontinuities, with minimal numerical dissipation and oscillations, has been a lasting challenge to the computational fluid dynamicist as well as to the numerical analyst since the advent of computers. The 1980s witnessed an explosive interest and research in upwind schemes for their capability of achieving high accuracy over a wide range of problems described by Euler or Navier–Stokes equations. Today, upwind schemes undoubtedly have become the main spatial discretization techniques adopted in nearly all major codes.

Roe in the survey paper [4] gives a comparative description of the upwind schemes developed in the early 80s, generally classified into the so-called flux-vector and flux-difference splittings, and points out their successes and failures. Quirk adds an interesting catalogue of situations denying several current Riemann solvers success [5].

The current research is motivated by the desire to achieve both the efficiency of the flux-vector splitting and the accuracy of the flux-difference splitting. Thus, a new breed of upwind schemes have been produced since the beginning of the 90s. To be practically useful, such a scheme should hold robustness/stability for a *wide* range of problems—Euler and Navier–Stokes equations, ideal and nonequilibrium gas, and steady and unsteady flows. Our recent attempts toward deriving a scheme meeting these goals have proven to be promising, resulting in two classes of schemes: (1) the so-called AUSM [1, 2] and its derivatives, such as AUSMDV [6] by Wada and Liou and the present AUSM$^+$ [3], and (2) the HUS [7–9] by Coquel and Liou. The AUSMDV, a blending form of AUSM, flux-difference, and flux-vector splittings, improves the robustness of AUSM in dealing with the collision of strong shocks. However, the "carbuncle phenomenon" appears, albeit much weaker than that resulting from the Roe scheme, and requires a fix. We suggest in [6] an effective procedure to cure the problem. The HUS (hybrid upwind splitting) scheme, endows the nonlinear field with a flux-vector splitting and the linear field with a low-diffusion scheme, such as the Roe and Osher schemes. Unfortunately, it also gives rise to the daunting "carbuncle phenomenon," even though it may be weak. Unlike AUSM$^+$, both AUSMDV and HUS schemes, however, do not have the exact property of capturing a stationary shock. The HUS is also more complicated and more expensive to compute than the other two.

Even though the original scheme, AUSM, enjoys remarkable success, its drawbacks also surface. In a continuing search for a near-perfect numerical flux scheme, we report in this paper recent progress toward this end. We aim at addressing some fundamental properties in terms of mathematical analysis. As a result, a new version, termed AUSM$^+$, has been derived and is shown in this paper to have the following features: (1) exact resolution of a stationary normal shock or contact discontinuity, (2) positivity-preserving property, and (3) improvement in accuracy over its predecessor AUSM and other popular schemes, (4) simplicity and easy generalization to other conservation laws. Shock resolution has been subject of considerable interest for theoretical as well as practical reasons. The relevance of resolving a contact discontinuity

0021-9991/96 $18.00

to accurate prediction of boundary/shear layer was convincingly demonstrated by Van Leer *et al.* [18]. Property (2) proves to be closely related to the robustness of the scheme for species calculation and flow in rapid acceleration, e.g., around a corner. The improvement in reliability/accuracy achieved by the AUSM$^+$ will become evident for a number of test cases included in the present paper.

This paper is organized as follows. In Section 2 we give preliminaries and a brief summary of the AUSM [1, 2]. In Section 3 we give development of the AUSM$^+$ and prove some relevant properties. We analyze in Section 4 the AUSM$^+$ numerical flux and compare it with other flux schemes. In Section 5 we stress the use of the pressure boundary condition derived from the characteristic relation. Higher order extension used in the context of AUSM$^+$ is briefly given in Section 6. We will discuss in Section 7 the results of several test cases, together with comparisons with other schemes. Finally a brief concluding remark is given.

2. PRELIMINARIES

Consider as an initial-value problem the one-dimensional (1D) system of conservation laws for ideal-gas flows,

$$\frac{\partial \mathbf{U}}{\partial t} + \frac{\partial \mathbf{F}}{\partial x} = 0, \quad t > 0, -\infty \le x \le \infty,$$
$$\mathbf{U}(x, 0) = \mathbf{U}_0(x), \tag{1}$$

where $\mathbf{U} = (\rho, \rho u, \rho e_t)^{\mathrm{T}}$ belongs to a phase space $\mathscr{U} \in \mathscr{R}^3$, the inviscid flux $\mathbf{F} = (\rho u, \rho u^2 + p, \rho u h_t)^{\mathrm{T}}$ denotes a smooth mapping $\mathbf{F}: \mathscr{U} \to \mathscr{R}^3$. We denote the specific total energy $e_t = e + u^2/2 = h_t - p/\rho$, and the ideal-gas equation of state is assumed, $p = (\gamma - 1)\rho e$, $\gamma = 1.4$.

For the numerical solution of (1), we shall consider piecewise constant approximations $\mathbf{U}_j^{n+1}$ defined by the explicit 3-point scheme in conservation form,

$$\mathbf{U}_j^{n+1} = \mathbf{U}_j^n - \lambda(\mathbf{f}_{j+1/2}^n - \mathbf{f}_{j-1/2}^n), \quad n \in N, j \in Z, \tag{2}$$

where $\lambda = \Delta t/\Delta x$, Δt and Δx being respectively the time and space steps. Here, the numerical flux defined by

$$\mathbf{f}_{j+1/2}^n = \mathbf{f}(\mathbf{U}_j^n, \mathbf{U}_{j+1}^n) \tag{3}$$

is assumed to be a Lipschitz continuous function and to satisfy the consistency condition:

$$\mathbf{f}(\mathbf{U}, \mathbf{U}) = \mathbf{F}(\mathbf{U}). \tag{4}$$

In the finite-volume formulation (2)–(3), the differences among all the numerical schemes lie essentially in the definition of the numerical flux $\mathbf{f}_{j+1/2}$ evaluated at the cell interface. The performance of the numerical flux will vary, depending on what set of properties it must meet.

As a first step in the formulation of the AUSM family of schemes, we recognize the convection and acoustic waves as two physically distinct processes and write the inviscid flux as a sum of the convective and pressure terms,

$$\mathbf{F} = \mathbf{F}^{(c)} + \mathbf{P}, \tag{5a}$$

where

$$\mathbf{F}^{(c)} = Ma \begin{pmatrix} \rho \\ \rho u \\ \rho h_t \end{pmatrix}, \quad \mathbf{P} = \begin{pmatrix} 0 \\ p \\ 0 \end{pmatrix}. \tag{5b}$$

Here the convective flux $\mathbf{F}^{(c)}$ is expressed in terms of the convective speed M and the passive scalar quantities indicated in the brackets. The pressure flux $\mathbf{P}$ contains nothing but the pressure term.

Let us first denote the convection used in the present paper. Boldface characters denote a column vector of variables defined at the continuous level, the lower-case boldface indicates the numerical flux at the discrete level, and the calligraphic type used for the split Mach number and pressure functions. Correspondingly we shall express the *numerical flux* $\mathbf{f}_{j+1/2}$ as the sum of the *numerical convective flux* $\mathbf{f}_{j+1/2}^{(c)}$ and the *numerical pressure flux,* at the interface $j + 1/2$ straddling the jth and $(j + 1)$th cells,

$$\mathbf{f}_{j+1/2} = \mathbf{f}_{j+1/2}^{(c)} + \mathbf{p}_{j+1/2}, \tag{6a}$$

where we further write

$$\mathbf{f}_{j+1/2}^{(c)} = m_{j+1/2}\Phi_{j+1/2} \tag{6b}$$

and

$$\mathbf{p}_{j+1/2} = \begin{pmatrix} 0 \\ p_{j+1/2} \\ 0 \end{pmatrix}. \tag{6c}$$

For the AUSM formulation [1], these interface quantities are summarized in the following: First we define $\forall j \in Z$,

$$m_{j+1/2} = \mathscr{M}_j^+ + \mathscr{M}_{j+1}^-, \quad \mathscr{M}_j^\pm = \mathscr{M}^\pm(M_j), \tag{7a}$$
$$p_{j+1/2} = \mathscr{P}_j^+ p_j + \mathscr{P}_{j+1}^- p_{j+1}, \quad \mathscr{P}_j^\pm = \mathscr{P}^\pm(M_j), \tag{7b}$$

where

$$\mathscr{M}^{\pm}(M) = \begin{cases} \frac{1}{2}(M \pm |M|), & \text{if } |M| > 1, \\ \pm\frac{1}{4}(M \pm 1)^2, & \text{otherwise;} \end{cases} \tag{8}$$

and

$$\mathscr{P}^{\pm}(M) = \begin{cases} \frac{1}{2}(1 \pm \text{sign}(M)), & \text{if } |M| \geq 1, \\ \frac{1}{4}(M \pm 1)^2(2 \mp M), & \text{otherwise.} \end{cases} \tag{9}$$

Then simple upwinding is applied to define $\Phi_{j+1/2}$:

$$\Phi_{j+1/2} = \begin{cases} \mathbf{\Phi}_j, & \text{if } m_{j+1/2} \geq 0, \\ \mathbf{\Phi}_{j+1}, & \text{otherwise;} \end{cases} \tag{10}$$

$\mathbf{\Phi} = (\rho a, \rho a u, \rho a h_t)^{\mathrm{T}}$.

Despite successes brought by the scheme, we have also found drawbacks and concluded that further improvement is warranted. In fact, it is possible to derive an improved scheme, termed AUSM$^+$ [3], which contains AUSM as a special case. In this new formulation, the two splittings reported in [1, 2] (respectively, in terms of Mach number and velocity) are unified and the scheme is capable of exactly capturing, not only a stationary contact discontinuity, but also a stationary shock. Furthermore, a set of more general Mach number and pressure splitting functions are used in the AUSM$^+$, resulting in improvement in accuracy, such as removing postshock overshoot and a glitch in the slowly moving shock problem (see respectively Problem 4 and case "E" in Problem 2 in Section 7). In what follows, we will present the detailed steps for constructing the AUSM$^+$ and give some interesting heretofore unreported mathematical properties that bear physical consequences. In particular, the positivity-preserving property that allows calculations of strong rarefaction and near vacuum flows.

3. AUSM$^+$

As we saw in the previous section, the AUSM scheme simply consists of two steps: (1) the definition of $\mathscr{M}^{\pm}$ and $\mathscr{P}^{\pm}$, followed by (2), a simple upwind selection advection of $\Phi_{j+1/2}$. In essence, we propose to deal with the genuinely *nonlinear* field associated with the eigenvalues $(u \pm a)$ in the first step and the *linearly* degenerate field associated with the eigenvalue (u) in the second step. In other words, the interface (numerical) velocity and pressure will be determined by considering the *nonlinear* field when we define their explicit functional forms.

The key for unifying the Mach number and velocity formulations [1, 2] is the notion of common speed of sound defined at the cell interface. This notion turns out to be very useful. It allows, in 1D stationary flow, the exact capturing of a contact discontinuity in the AUSMDV [6] and, in addition, the exact capturing of a shock wave in the AUSM$^+$.

Let the common speed of sound be denoted by $a_{j+1/2}$. We now rewrite the numerical convective flux in (6b) as

$$\mathbf{f}^{(c)}_{j+1/2} = m_{j+1/2} a_{j+1/2} \Phi_{j+1/2}, \quad \mathbf{\Phi} = (\rho, \rho u, \rho h_t)^{\mathrm{T}}. \tag{11}$$

We note that the quantity $\mathbf{\Phi}$ in (11) differs by a factor a from that used in the AUSM, as shown in (10), and we shall solely use the former hereafter in the paper. The scalar quantities in $\Phi_{j+1/2}$ again are given by the simple upwinding (10), with the content of $\mathbf{\Phi}$ now given in (11). What remains is to define $(m_{j+1/2}, p_{j+1/2})$ and $a_{j+1/2}$ for which we shall develop the detailed framework in the following.

3.1. *Definition of* $(m_{j+1}, p_{j+1/2})$

Anticipating contributions from "j" and "$j+1$" states to the interface Mach number $m_{j+1/2}$, let us write for a 3-point scheme the mapping $m: \mathscr{U} \times \mathscr{U} \to \mathscr{U} \in \mathscr{R}$,

$$m_{j+1/2} = m(M_j, M_{j+1}). \tag{12}$$

Specifically we write $m_{j+1/2}$ as a sum of two individual components,

$$m_{j+1/2} = \mathscr{M}^{+}(M_j) + \mathscr{M}^{-}(M_{j+1}), \tag{13}$$

where the superscripts "+" and "−" are understood to be associated with the right- and left-running waves.

For 1D conservation laws, the nonlinear characteristic equations are

$$dp \pm \rho a du = 0, \quad \text{along } \frac{dx}{dt} = u \pm a. \tag{14}$$

This simply suggests that the velocity and pressure are closely coupled and that the characteristic variables expressed in (14) are propagating locally at the speeds $u \pm a$. For $|M| < 1$, the two waves move in opposite directions and interact with each other. Hence the interface velocity and pressure, composed of the interaction of these two waves, are constructed using $(u \pm a)$ as basis functions in the polynomial expansion. This suggests the following expansion in terms of $(M \pm 1)$:

$$\mathscr{M}^{\pm} = \tfrac{1}{2}(M \pm 1) \quad \text{for } |M| < 1. \tag{15}$$

This in fact is a form of eigenvalue expansion, utilizing just the eigenvalues associated with the genuinely nonlinear fields. Then from (13), the interface Mach number is defined, as $|M| < 1$, by

$$m_{j+1/2} = \tfrac{1}{2}[(M+1)_j + (M-1)_{j+1}]. \tag{16}$$

This in fact corresponds to the simple average of M_j and M_{j+1}. As in the Van Leer splitting [11], the present method makes explicit use of the eigenvalues associated with the nonlinear waves, $M \pm 1$. Using the eigenvalues as a basis for expressing the numerical fluxes is quite common in the upwind formulation. For example, it comes naturally in the Steger–Warming and Roe fluxes as the Jacobian matrix is explicitly expressible in terms of its eigenvalues. Specifically, Steger-Warming splitting [10] begins by grouping $\mathbf{F}$ as:

$$\mathbf{F} = \frac{\rho}{2\gamma}\left\{(u+a)\begin{pmatrix}1\\ u+a\\ H+ua\end{pmatrix} + (u-a)\begin{pmatrix}1\\ u-a\\ H-ua\end{pmatrix} + 2(\gamma+1)u\begin{pmatrix}1\\ u\\ u^2/2\end{pmatrix}\right\}. \tag{17}$$

Similar explicit expansion can be found for the flux difference in the Roe scheme.

To remove the nondifferentiability of (15) when the sign of eigenvalues changes, Van Leer [11] chose differentiable, second-order polynomials:

$$\mathscr{M}^{\pm} = \pm\tfrac{1}{4}(M \pm 1)^2. \tag{18}$$

It is evident that the above split formula (18) results in an unsymmetric distribution of signals propagated by the characteristic speeds ($M \pm 1$) as $M \neq 0$ and becomes the simple (symmetric) average as M tends to zero, leading to the formula used commonly in the pressure-based codes for incompressible flows.

In the present study, we present a more general footing for designing the split formulas. First we require that the split Mach number and pressure functions satisfy the following properties listed in Propositions 3.1 and 3.2.

PROPOSITION 3.1. *Let the split Mach numbers $\mathscr{M}^{\pm}$ be chosen such that they hold the following properties*:

- [M1] $\mathscr{M}^+(M) + \mathscr{M}^-(M) = M$, *for consistency*.
- [M2] $\mathscr{M}^+(M) \geq 0$ *and* $\mathscr{M}^-(M) \leq 0$.
- [M3] $\mathscr{M}^{\pm}$ *are monotone increasing functions of* M.
- [M4] $\mathscr{M}^+(M) = -\mathscr{M}^-(-M)$, *i.e., a symmetry property*.
- [M5] $\mathscr{M}^+(M) = M$ *as* $M \geq 1$; $\mathscr{M}^-(M) = M$ *as* $M \leq -1$.
- [M6] $\mathscr{M}^{\pm}$ are continuously differentiable.

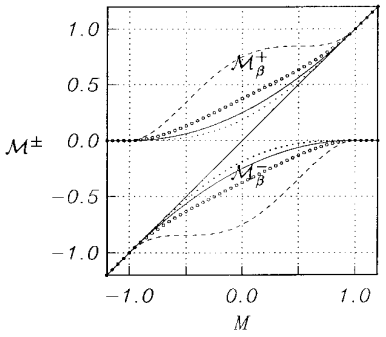

FIG. 1. $\mathscr{M}^{\pm}$ vs M; solid line: $\beta = 0$, ...: $\beta = -\frac{1}{16}$, −− : $\beta = \frac{1}{2}$, ○○ : $\beta = \frac{1}{8}$.

Consequently we have the following results.

LEMMA 3.1. *Let $m_{j+1/2}$ be defined as in* (13), *then* (1) $m_{j+1/2} \in [M_j, M_{j+1}]$, $j \in Z$, *and* (2) $0 < \mathscr{M}^+ < 1$ *and* $0 > \mathscr{M}^- > -1$ *as* $|M| < 1$.

Proof. Let $D = (m_{j+1/2} - M_j)(m_{j+1/2} - M_{j+1})$, substituting (13) and [M1] in D gives

$$D = -(\mathscr{M}^-(M_j) - \mathscr{M}^-(M_{j+1}))(\mathscr{M}^+(M_j) - \mathscr{M}^+(M_{j+1})) \leq 0,$$

where the product of two parentheses is nonnegative by virtue of [M3]. From [M2], [M3], and [M5], statement (2) immediately follows. ∎

DEFINITION OF $\mathscr{M}^{\pm}$. The split Mach numbers $\mathscr{M}^{\pm}$,

$$\mathscr{M}^{\pm}(M) = \begin{cases}\tfrac{1}{2}(M \pm |M|), & \text{if } |M| \geq 1,\\ \mathscr{M}^{\pm}_{\beta}(M), & \text{otherwise,}\end{cases} \tag{19a}$$

with

$$\mathscr{M}^{\pm}_{\beta}(M) = \pm\tfrac{1}{2}(M \pm 1)^2 \pm \beta(M^2-1)^2, \quad -\tfrac{1}{16} \leq \beta \leq \tfrac{1}{2}, \tag{19b}$$

satisfy the properties [M1]–[M6].

Figure 1 displays the distribution of $\mathscr{M}^{\pm}(M)$ with various values of β; the polynomials $\mathscr{M}^{\pm}_{\beta=0}$ correspond to the Van Leer formula [11] and are the lowest degree polynomials differentiable at $M = \pm 1$.

Next, the interface pressure for a 3-point flux scheme is written in general as

$$p_{j+1/2} = p(M_j, p_j, M_{j+1}, p_{j+1}), \tag{20a}$$

or specifically,

$$p_{j+1/2} = \mathscr{P}^+(M_j)p_j + \mathscr{P}^-(M_{j+1})p_{j+1}. \tag{20b}$$

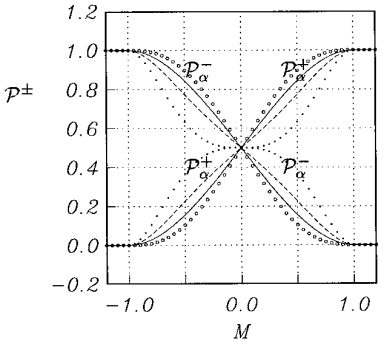

FIG. 2. $\mathscr{P}^{\pm}$ vs M; solid line: $\alpha = 0$, ...: $\alpha = -\frac{3}{4}$, $--$: $\alpha = -\frac{1}{4}$, $\circ\circ$: $\alpha = \frac{3}{16}$.

PROPOSITION 3.2. *We require that the split pressures* $\mathscr{P}^{\pm}$ *satisfy the following properties*:

[P1] $\mathscr{P}^{+}(M) + \mathscr{P}^{-}(M) = 1$, *for consistency*.

[P2] $0 \le \mathscr{P}^{\pm}(M)$, *as required by the physical constraint that the pressure be nonnegative*.

[P3] $\partial\mathscr{P}^{+}/\partial M \ge 0$ *and* $\partial\mathscr{P}^{-1}/\partial M \le 0$.

[P4] $\mathscr{P}^{+}(M) = \mathscr{P}^{-}(-M)$.

[P5] $\mathscr{P}^{+} = 1$ *as* $M > 1$; $\mathscr{P}^{-} = 1$ *as* $M < -1$.

[P6] $\mathscr{P}^{\pm}(M)$ are continuously differentiable.

Similar assertion can be made about the pressure splitting as for the Mach number.

LEMMA 3.2. *If the data* $p_j > 0$ $\forall j \in Z$, *then* (1) $p_{j+1/2}$ *remains positive and lies in* $[0, p_j + p_{j+1}]$, (2) $p_{j+1/2}$ *is a monotone function of both* p_j *and* p_{j+1} *and is monotone increasing in* M_j *but decreasing in* M_{j+1}, *and* (3) $\mathscr{P}^{\pm}(M) \le 1$ $\forall M \in \mathscr{R}$.

Proof. The proof of (1) follows directly by virtue of [P2]. Since $p_{j+1/2}$ as expressed in (20b) is function of four variables, one quickly proves the second and third statements by using [P2] and [P3], and [P5], respectively. ∎

DEFINITION OF $\mathscr{P}^{\pm}$. The split pressures

$$\mathscr{P}^{\pm}(M) = \begin{cases} \frac{1}{2}(1 \pm \text{sign}(M)), & \text{if } |M| \ge 1, \\ \mathscr{P}^{\pm}_{\alpha}(M), & \text{otherwise.} \end{cases} \tag{21a}$$

with

$$\mathscr{P}^{\pm}_{\alpha}(M) = \tfrac{1}{4}(M \pm 1)^2(2 \mp M) \pm \alpha M(M^2 - 1)^2, \quad -\tfrac{3}{4} \le \alpha \le \tfrac{3}{16}, \tag{21b}$$

hold [P1]–[P6]. The $\mathscr{P}^{\pm}$ versus M curves as shown in Fig. 2.

Next we consider the criteria for setting the values of the parameters (α, β). It is noted that there exists an inflection point in $\mathscr{P}^{\pm}_{\alpha}$ at $M = 0$ $\forall\alpha$. Thus, if we also allow in $\mathscr{M}^{\pm}_{\beta}$ the same inflection point at $M = 0$, and no other additional inflections in $\mathscr{P}^{\pm}_{\alpha}$ for $M \in [-1, 1]$, except at the end points $M = \pm 1$, then we get the following results.

LEMMA 3.2.

$$\frac{d^2\mathscr{M}^{\pm}_{\beta}}{dM^2}(0) = 0, \quad \Rightarrow \beta = \frac{1}{8}, \tag{22a}$$

$$\frac{d^2\mathscr{P}^{\pm}_{\alpha}}{dM^2}(\pm 1) = 0, \quad \Rightarrow \alpha = \tfrac{3}{16}. \tag{22b}$$

The curves corresponding to these values are included in Figs. 1 and 2, respectively. These values are recommended for use because this pair have given results that are improved over the AUSM and comparable with the Roe splitting. While the above criteria may seem intuitive and there might be a better choice, they have nevertheless performed well on many calculations, including those presented in the paper. Figure 3 displays the first-order solutions obtained using the Roe and AUSM^{+} with $\alpha = \beta = 0$ and $(\alpha, \beta) = (\frac{3}{16}, \frac{1}{8})$ as given in (22), clearly showing the advantage of using the additional higher-degree terms in $(\mathscr{P}^{\pm}_{\alpha}, \mathscr{M}^{\mp}_{\beta})$ and the accuracy comparable to that of the Roe splitting. We note that the first-order solution is very meaningful for judging the performance of a scheme, for it reveals the sheer accuracy of the scheme. It is also fundamental because the higher-order scheme is built up from the first-order one. However, higher order accurate solutions are more useful in practice; hence we discuss higher order extension in Section 6 and present the second-order accurate results in Section 7.

3.2. *Definition of* $a_{j+1/2}$

To achieve the unification of the velocity and Mach number ($c = u$, M) splittings [1, 2], it is obvious that we can no longer use each respective speed of sound, a_j or a_{j+1}, but instead should use a common one. The notion of the common speed of sound, also employed in [6], turns out to be very useful. It allows, in 1D stationary flow, the exact capturing of the contact discontinuity in AUSMDV [6] and, in addition, the exact capturing of the shock wave in AUSM^{+}. This is also justifiable from the physical point of view. Since the interface flux is viewed as a recipient of contributions from both neighboring cells, it certainly makes sense to use a common speed of sound defined there as a basis for determining the Mach number and subsequent upwinding. Let us now write

$$a_{j+1/2} = a(\mathbf{U}_j, \mathbf{U}_{j+1}). \tag{23}$$

It is this freedom that allows us to make a favorable choice to attain an exact capture of a stationary shock.

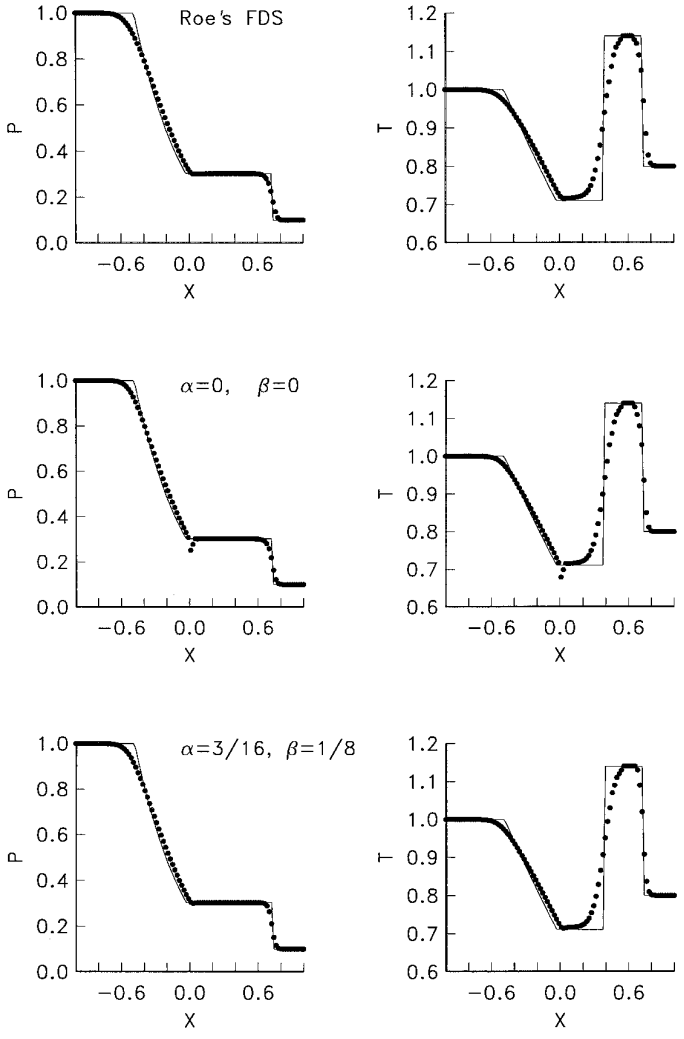

FIG. 3. Shock tube (Sod) problem; first-order solutions by the Roe (top), and AUSM$^+$ schemes $\alpha = \beta = 0$ (middle) and $(\alpha, \beta) = (\frac{3}{16}, \frac{1}{8})$ (bottom).

It is of interest to note that we can write $a_{j+1/2}$ for AUSM in the present AUSM$^+$ formulation:

$$a_{j+1/2} = \begin{cases} a_j, & \text{if } m_{j+1/2} \geq 0, \\ a_{j+1}, & \text{otherwise.} \end{cases} \tag{24}$$

Thus, AUSM belongs to a special case of AUSM$^+$.

LEMMA 3.3. *Consider a* 1*D stationary shock problem*:

$$\mathbf{U} = \begin{cases} \mathbf{U}_L, & x \leq x_j, \\ \mathbf{U}_R, & x > x_j, \end{cases} \tag{25}$$

where $\mathbf{U}_L$ and $\mathbf{U}_R$ are related via the normal shock relation and $u_j > a_j$. Let a_j^* be the critical speed of sound evaluated at U_j $(=\mathbf{U}_L)$, then the speed of sound used in the AUSM$^+$,

$$a_{j+1/2} = a_j^{*2}/u_j, \tag{26}$$

allows an exact resolution of the stationary shock for any (α, β) in (19) and (21).

Remark. The critical speed of sound a^* is calculated via the isoenergetic condition,

$$h_t = \frac{a^2}{\gamma - 1} + \frac{1}{2}u^2 = \frac{(\gamma + 1)a^{*2}}{2(\gamma - 1)} \quad \text{for ideal gas.} \tag{27}$$

It is well known that the Mach numbers based on the speeds of sound a and a^* indicate equally whether the flow lies at the sonic or the supersonic or the subsonic regime [12]. Namely, let $M = u/a$ and $M^* = u/a^*$; then

$$M = 1 \Leftrightarrow M^* = 1, \quad M > 1 \Leftrightarrow M^* > 1, \quad M < 1 \Leftrightarrow M^* < 1. \tag{28}$$

Hence, the critical speed of sound defined above can be used as a reference to define the Mach number to be used as the variable for upwinding.

Proof of Lemma 3.3. Referring to Fig. 4, we consider at most one intermediate (numerical) state "i" between the "L" and "R" states.

Let us now express the numerical flux at the interfaces (denoted here respectively by $\mp\frac{1}{2}$) enclosing the intermediate cell i. In order to explicitly include the undefined speed of sound, we opt for using the velocity splitting. Similar to (7a) (or referring to [2]), we write

$$u_{-1/2} = u_L^+ + u_i^- = a_{-1/2}(\mathscr{M}^+(M_L) + \mathscr{M}^-(M_i)). \tag{29}$$

Assuming $M_L > 1$ and $M_i < 1$ without loss of generality (since there must be a subsonic point connecting the supersonic point in the case of normal shock) and substituting property [M1] $\mathscr{M}^-(M_i) = (M_i - \mathscr{M}^+(M_i))$ and (19b) in (29) gives

$$u_{-1/2} = u_L - (u_i - a_{-1/2})^2 g^+(u_i, a_{-1/2}), \tag{30}$$

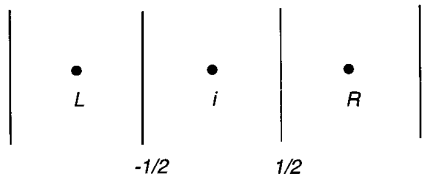

FIG. 4. One intermediate shock cell between "L" and "R."

where we define

$$g^{\pm}(u,a)=\frac{1}{4a}\left(1+4\beta\left(\frac{u}{a}\pm 1\right)^2\right). \tag{31}$$

It is easy to show $u_{-1/2}>0$ as $u_L>u_i$; hence by (6) we get

$$\mathbf{f}_{-1/2}=\begin{pmatrix}\dot{m}_{-1/2}\\ u_L\dot{m}_{-1/2}+p_{-1/2}\\ h_{tL}\dot{m}_{-1/2}\end{pmatrix},\quad \dot{m}_{-1/2}=\rho_L u_{-1/2}. \tag{32}$$

This flux must be balanced with $\mathbf{F}_L$ as the "L" state is fixed. Hence, a simple algebra yields

$$\begin{pmatrix}u_{-1/2}\\ p_{-1/2}\end{pmatrix}=\begin{pmatrix}u_L\\ p_L\end{pmatrix}. \tag{33}$$

These two conditions can be satisfied exactly, for any (ρ_i, p_i), by requiring only one condition:

$$u_i=a_{-1/2}. \tag{34}$$

Let us now turn to the "$\frac{1}{2}$" face. The interface velocity becomes

$$u_{1/2}=(u_i+a_{1/2})^2g^-(u_i,a_{1/2})-(u_R-a_{1/2})^2g^+(u_R,a_{1/2})>0. \tag{35}$$

The inequality holds as $u_i>u_R$ is expected. Again substituting in (6) yields

$$\mathbf{f}_{1/2}=\begin{pmatrix}\dot{m}_{1/2}\\ u_i\dot{m}_{1/2}+p_{1/2}\\ h_{ti}\dot{m}_{1/2}\end{pmatrix},\quad \dot{m}_{1/2}=\rho_i u_{1/2}. \tag{36}$$

In order to eliminate this intermediate state, we let

$$\mathbf{U}_i=\mathbf{U}_R,\quad \text{or}\quad \begin{pmatrix}u_i\\ \rho_i\\ p_i\end{pmatrix}=\begin{pmatrix}u_R\\ \rho_R\\ p_R\end{pmatrix}. \tag{37}$$

It turns out that the last two requirements in the above equation respectively for ρ_i and p_i are automatically satisfied if (34) and the first requirement, $u_R=u_i$, are set. Thus,

$$a_{-1/2}=u_R=u_i. \tag{38}$$

This requirement in fact enforces the conservation of fluxes by relating the upstream supersonic "L" state to the downstream subsonic "R" state. It is desirable to express $a_{-1/2}$ in terms of the upstream state "L." In fact, the well-known Prandtl relation (see, for example, [12]) is at hand for use,

$$u_Ru_L=a_L^{*2}=a_R^{*2}=\frac{2}{\gamma+1}a_t^2, \tag{39}$$

where a_t is the speed of sound based on the total enthalpy h_t. Putting $L\to j$ and $R\to j+1$, we get (26). And since the above algebra is independent of specific values of (α, β), the proof now is complete. ▮

Note that the formula (26) is valid for $u_L>a_L^*$. We now must extend it to other conditions such as subsonic speed or $u_L<0$; we suggest the following formula for $M\in\mathscr{R}$:

$$a_{j+1/2}=\min(\tilde{a}_L,\tilde{a}_R),\quad \tilde{a}=a^{*2}/\max(a^*,|u|). \tag{40}$$

That is, $\tilde{a}$ is taken to be a^* when $|u|<a^*$.

In Fig. 5 we show the numerical result for a single stationary shock discontinuity. The present AUSM$^+$, like Roe splitting, produces the exact solution. In contrast, the AUSM and Van Leer splittings (not shown) resolve the shock with two intermediate points [11]. However, when the specific speed of sound (Eq. (26)) is used in the Van Leer–Hänel splitting [15], an exact shock is astonishingly reproduced.

Other formulas may be used for the reason of simplicity, but at the expense of losing the above property. Some obvious choices are

$$a_{j+1/2}=\tfrac{1}{2}(a_j+a_{j+1}), \tag{41a}$$

$$a_{j+1/2}=\sqrt{a_ja_{j+1}}. \tag{41b}$$

In summary, the above splittings for both the advective and pressure terms completely define the Euler numerical flux. The AUSM$^+$ algorithm can be simply summarized as follows:

Let j and $j+1$ states be given, then

(A1) $M_j=u_j/a_{j+1/2}$, and $M_{j+1}=u_{j+1}/a_{j+1/2}$ via (40),

(A2) $m_{j+1/2}=\mathscr{M}^+(M_j)+\mathscr{M}^{-1}(M_{j+1})$, and $m^{\pm}_{j+1/2}=\frac{1}{2}(m_{j+1/2}\pm|m_{j+1/2}|)$, $p_{j+1/2}=\mathscr{P}^+(M_j)p_j+\mathscr{P}^-(M_{j+1})p_{j+1}$,

(A3) $$\mathbf{f}_{j+1/2}=a_{j+1/2}\left\{m^+_{j+1/2}\begin{pmatrix}\rho\\ \rho u\\ \rho h_t\end{pmatrix}_j+m^-_{j+1/2}\begin{pmatrix}\rho\\ \rho u\\ \rho h_t\end{pmatrix}_{j+1}\right\}+\begin{pmatrix}0\\ p_{j+1/2}\\ 0\end{pmatrix}.$$

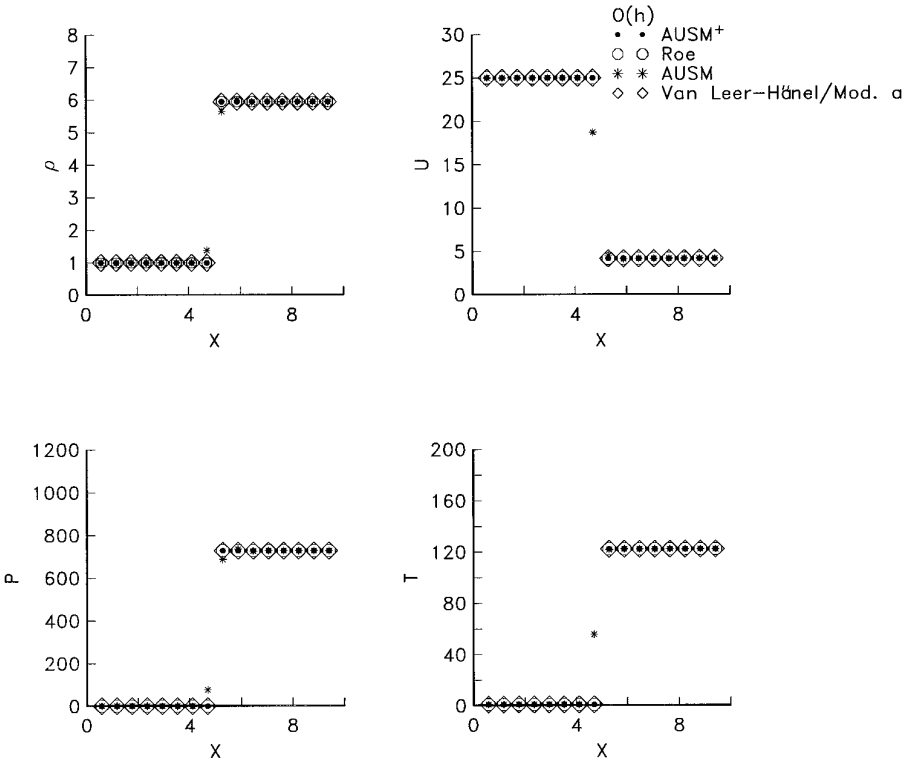

FIG. 5. Stationary shock, $M_L = 25$.

4. ANALYSIS OF AUSM+

The numerical flux defined above can be rewritten as

$$\mathbf{f}_{j+1/2} = a_{j+1/2}\left[\tfrac{1}{2}m_{j+1/2}(\mathbf{\Phi}_j + \mathbf{\Phi}_{j+1}) - \tfrac{1}{2}|m_{j+1/2}|(\mathbf{\Phi}_{j+1} - \mathbf{\Phi}_j)\right] + \mathbf{p}_{j+1/2}, \tag{42}$$

where Φ is defined in (11) and $(a, m, p)_{j+1/2}$ are defined in Section 3.1. Several observations are in order.

The first term on the RHS is clearly not a simple average of "j" and "$j + 1$" states, but rather a Mach number-weighted average. The dissipation coefficient $|m_{j+1/2}|$ is merely a *scalar* as opposed to a matrix, thus requiring only $O(n)$ operations, where n is the number of equations to be solved.

The present scheme does not involve differentiation, specifically the Jacobian matrix, in the evaluation of $\mathbf{f}_{j+1/2}$. Since $m_{j+1/2}$ says nothing about the dimension of $\mathbf{f}$, the AUSM schemes are readily extendable to a general equation of state and to chemical and thermal nonequilibrium flows [29, 30] or to turbulence model equations. All it takes is to append additional conservation equations using the same convective speed $m_{j+1/2}$. Again, the cost is only linearly increased with the additional conservation equations considered. In the case of the Roe or Osher scheme in which the Jacobian matrix is essential, there is a need for redefining the averaged/intermediate states as additional equations are included, which can become somewhat tricky.

Next, we write well-known numerical fluxes in a form similar to (42) for comparison. Let $\Delta_{j+1/2}(\ ) = (\ )_{j+1} - (\ )_j$:

Roe [13],

$$\mathbf{f}_{j+1/2} = \tfrac{1}{2}[(u\mathbf{\Phi})_j + (u\mathbf{\Phi})_{j+1}] - \tfrac{1}{2}|\mathbf{A}(\hat{\mathbf{U}})|\,\Delta_{j+1/2}\mathbf{U} + \tfrac{1}{2}(\mathbf{P}_j + \mathbf{P}_{j+1}), \tag{43a}$$

where $\hat{\mathbf{U}}$ is the Roe-averaged state and $|\mathbf{A}| = \mathbf{A}^+ - \mathbf{A}^-$ in the usual sense.

Osher–Solomon[14],

$$\mathbf{f}_{j+1/2} = \frac{1}{2}[(u\mathbf{\Phi})_j + (u\mathbf{\Phi})_{j+1}] - \frac{1}{2}\int_{\mathbf{U}_j}^{\mathbf{U}_{j+1}} |\mathbf{A}(\mathbf{U})|\,\mathbf{dU} + \frac{1}{2}(\mathbf{P}_j + \mathbf{P}_{j+1}). \tag{43b}$$

Steger–Warming [10],

$$\mathbf{f}_{j+1/2} = \tfrac{1}{2}[(u\mathbf{\Phi})_j + (u\mathbf{\Phi})_{j+1}] - \tfrac{1}{2}\,\Delta_{j+1/2}|\mathbf{A}|\mathbf{U} + \tfrac{1}{2}(\mathbf{P}_j + \mathbf{P}_{j+1}). \tag{43c}$$

Van Leer–Hänel [11, 15],

$$\mathbf{f}_{j+1/2} = \tfrac{1}{2}[(Ma\mathbf{\Phi})_j + (Ma\mathbf{\Phi})_{j+1}] - \tfrac{1}{2}\Delta_{j+1/2}a|\mathscr{M}|\mathbf{\Phi} + \mathbf{p}_{j+1/2}, \quad |\mathscr{M}| = \mathscr{M}^+ - \mathscr{M}^-. \tag{43d}$$

It is noted in (43d) that the present notation $\mathscr{M}^\pm$, rather than $M^\pm$ as in [11], is used for the convective dissipation flux. Also $\beta = 0$ could be set in $\mathscr{M}^\pm$ if the Van Leer formula were strictly adopted.

The Steger–Warming and Roe splittings differ only in the evaluation of the absolute Jacobian. This absolute Jacobian for the latter is evaluated at the well-known "Roe-average" state using *both* the "j" and "$j + 1$" states and is taken *outside* of the difference operator. In fact, this comparison reveals clearly that a striking difference in form between the FVS and FDS lies in *whether the dissipation matrix* (*or scalar*) *is differenced*. In this regard, the present scheme may appear formally close to a FDS, but it differs in the averaged term. On the other hand, the method retains the efficiency of the Van Leer scheme in defining the dissipation term. Consequently, the present scheme is neither FDS nor FVS, but rather a hybrid one.

As an aside, the Roe flux difference scheme expressed as $\Delta\mathbf{f} = |\mathbf{A}(\hat{\mathbf{U}})|\,\Delta\mathbf{U}$ may be interpreted as a formal application of the mean-value theorem with the exact definition of the mean (average) state, $\hat{\mathbf{U}} = \mathbf{U}(\mathbf{U}_j, \mathbf{U}_{j+1})$. This idea also turns out to be useful in the following section.

4.1. *Derivation of Jameson's CUSP Scheme* [25]

The above observation, moreover, suggests that we may make a quick alternative to the dissipation term in the Van Leer–Hänel formula (43d), by taking the term—$|\mathscr{M}| = \mathscr{M}^+ - \mathscr{M}^-$—out of the difference operator in order to mimic the flux-difference splitting. That is, we rewrite the diffusive term in (43d) as

$$\Delta_{1/2}(|\mathscr{M}|a\mathbf{\Phi}) = |\mathscr{M}|(\tilde{M})a_{1/2}\,\Delta_{j+1/2}\mathbf{\Phi}, \tag{44}$$

where $\tilde{M} = \tilde{M}(\mathbf{U}_j, \mathbf{U}_{j+1})$. And the function $|\mathscr{M}|(M)$, using the polynomials in (19), becomes

$$|\mathscr{M}|(M) = \begin{cases} |M|, & \text{if } |M| \geq 1, \\ \tfrac{1}{2}(M^2+1) + 2\beta(M^2-1)^2, & \text{otherwise.} \end{cases} \tag{45}$$

Next we rewrite the AUSM$^+$ pressure flux by using [P1] in Eq. (20b),

$$2p_{j+1/2} = (p_j + p_{j+1}) - (\mathscr{P}^+(M_{j+1}) - \mathscr{P}^-(M_{j+1}))p_{j+1} + (\mathscr{P}^+(M_j) - \mathscr{P}^-(M_j))p_j = (p_j + p_{j+1}) - \delta p_{j+1/2}, \tag{46}$$

where we let

$$\Delta\mathscr{P}(M) = \mathscr{P}^+(M) - \mathscr{P}^-(M) \tag{47a}$$

and

$$\delta p_{j+1/2} = \Delta\mathscr{P}(M_{j+1})p_{j+1} - \Delta\mathscr{P}(M_j)p_j. \tag{47b}$$

The above $\delta p_{j+1/2}$ is the diffusive term responsible for rendering the centered average upwinded. Substitution of (21) results in the simple formula:

$$\Delta\mathscr{P}(M) = \begin{cases} \operatorname{sign}(M), & \text{if } |M| \geq 1, \\ \dfrac{M}{2}\{3 - M^2 + 4\alpha(M^2-1)^2\}, & \text{otherwise.} \end{cases} \tag{48}$$

Again, we define a mean value $\hat{M}(M_j, M_{j+1}, p_j, p_{j+1})$ such that

$$\delta p_{j+1/2} = \Delta\mathscr{P}(\hat{M})(p_{j+1} - p_j). \tag{49}$$

Here $\hat{M}$ need not be equal to $\tilde{M}$ defined in (44). We now arrive at the dissipation fluxes—Eqs. (44) and (49)—recently proposed by Jameson [25] in the CUSP scheme, by setting a parameter a_o in his scheme, $a_o = 2\beta + \frac{1}{2}$ and $\alpha = 0$. We note that the added fluxes can be regarded as an enhanced and a FDS variation of the Van Leer flux vector splitting, (43d); it is however an approximate one to the AUSM$^+$ because $|\mathscr{M}|(\tilde{M})$ is not equal to $|m_{j+1/2}|$. Unfortunately, this formula does not preserve contact discontinuity unless $a_o = 0$. But for capturing shocks, this constant a_o needs to be adjusted and it is in general problem-dependent. Furthermore, there is an issue concerning the proper definition of the averaged Mach number $\tilde{M}$ and $\hat{M}$.

In order to get the full version of the AUSM$^+$ from the central averaging scheme, additional steps are required, which we shall discuss later in Section 4.2.

We now proceed to prove some interesting numerical properties of the present scheme. For the sake of algebraic clarity, we choose in the analysis to use the variable u, instead of M, but we recall that they are interchangeable in the formulation of AUSM$^+$. That is, for the $(j + \frac{1}{2})$ face,

$$u_{j+1/2} = a_{j+1/2}m_{j+1/2}, \tag{50a}$$

$$u^\pm_{j+1/2} = (u_{j+1/2} \pm |u_{j+1/2}|)/2. \tag{50b}$$

LEMMA 4.1. *The present splitting preserves the stationary contact discontinuity.*

Proof. Let $p_j = p_{j+1} = p$, $u_j = u_{j+1} = 0$, and $\rho_j \neq \rho_{j+1}$ across the stationary contact. We get $\mathscr{M}^+(0) = -\mathscr{M}^-(0)$

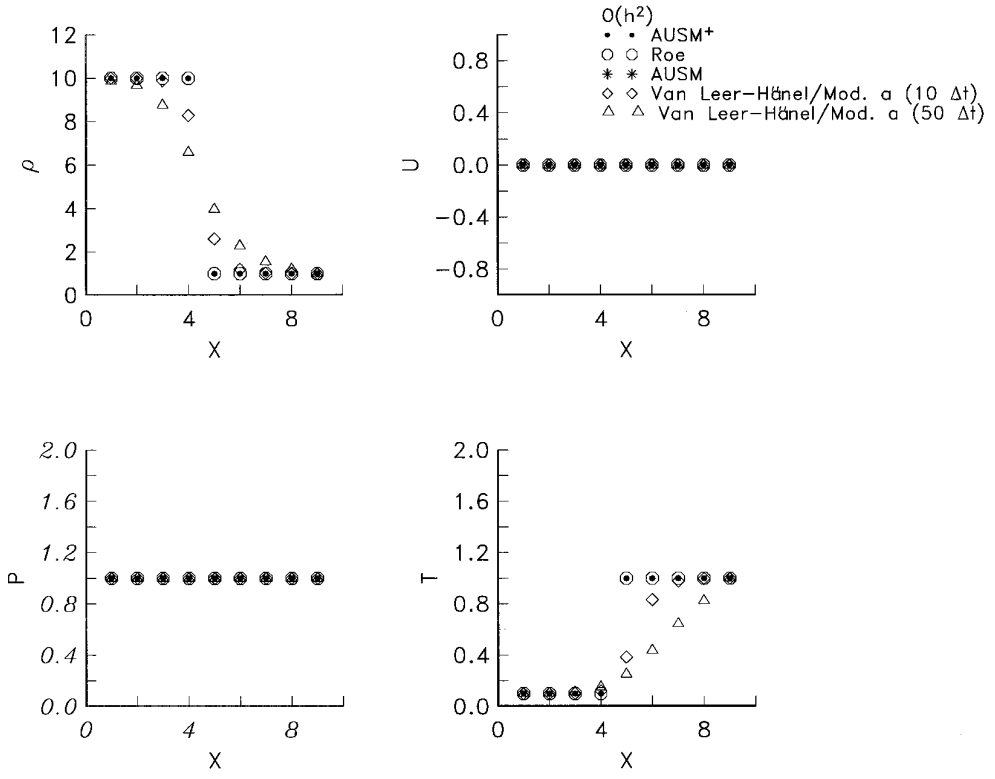

FIG. 6. Stationary contact discontinuity.

and $\mathscr{P}(0) = \mathscr{P}^-(0)$. Hence, $m_{j+1/2} = u_{j+1/2} = 0$, and $p_{j+1/2} = p$, yielding $\mathbf{f}_{j+1/2} = (0, p, 0)\ \forall j$. Thus, $\partial \mathbf{U}/\partial t = 0$, and the flow remains stationary and the contact discontinuous. ▮

Figure 6 shows that both the Roe and AUSM$^+$ (also the AUSM) splittings give rise to exact solution of a stationary discontinuity. The Van Leer splitting increasingly smears the discontinuity as calculation continues, even with the modification using the common speed of sound defined in (40) which (as shown in Fig. 5) permits the Van Leer splitting to resolve the stationary shock exactly.

LEMMA 4.2. For steady flows, the present scheme preserves the constancy of total enthalpy.

Proof. Assuming without loss of generality a unidirectional flow, e.g., $u > 0$, the discrete continuity equation yields for steady flow, $u^+_{j+1/2}\rho_j - u^+_{j-1/2}\rho_{j-1} = 0$. And the energy equation gives $u^+_{j+1/2}\rho_j h_{tj} - u^+_{j-1/2}\rho_{j-1}h_{tj-1} = 0$. Hence, we find $h_{tj} = h_{tj-1} = \cdots = h_{t0}\ \forall j$, and the proof is complete. ▮

We note that this property is not satisfied by many upwind schemes, including those by Godunov, Roe, Osher, Steger–Warming, and Van Leer. To our knowledge, only those which upwind the unsplit form of the total enthalpy will preserve this quantity (e.g., [1–3, 6, 15]).

In what follows, we shall study the positivity-preserving property in the same fashion as analyzed by Larrouturou [16].

LEMMA 4.3. Under the CFL-like condition,

$$0 \le \lambda[u^+_{j+1/2} + (-u^-_{j-1/2})] \le 1, \quad \lambda = \Delta t/\Delta x, \tag{51}$$

the scheme preserves positivity of density, namely, for $\rho^0_j > 0\ \forall j$, we have

$$\rho^n_j \ge 0, \quad n > 0 \quad \forall j. \tag{52}$$

Proof. The mass conservation yields for $j \in Z$,

$$\rho^{n+1}_j = \rho^n_j - \lambda(f^n_{\rho,j+1/2} - f^n_{\rho,j-1/2}), \quad f_\rho = \rho u, \tag{53a}$$

where

$$f^n_{\rho,j+1/2} = u^+_{j+1/2}\rho^n_j + u^-_{j+1/2}\rho^n_{j+1}. \tag{53b}$$

Substituting and rewriting,

$$\begin{aligned}\rho^{n+1}_j = {} & \lambda u^+_{j-1/2}\rho^n_{j-1} + [1 - \lambda(u^+_{j+1/2} - u^-_{j-1/2})]\rho^n_j \\ & + (-\lambda u^-_{j+1/2})\rho^n_{j+1} = f(\rho^n_{j-1}, \rho^n_j, \rho^n_{j+1}; u_{j-1/2}, u_{j+1/2}).\end{aligned} \tag{54}$$

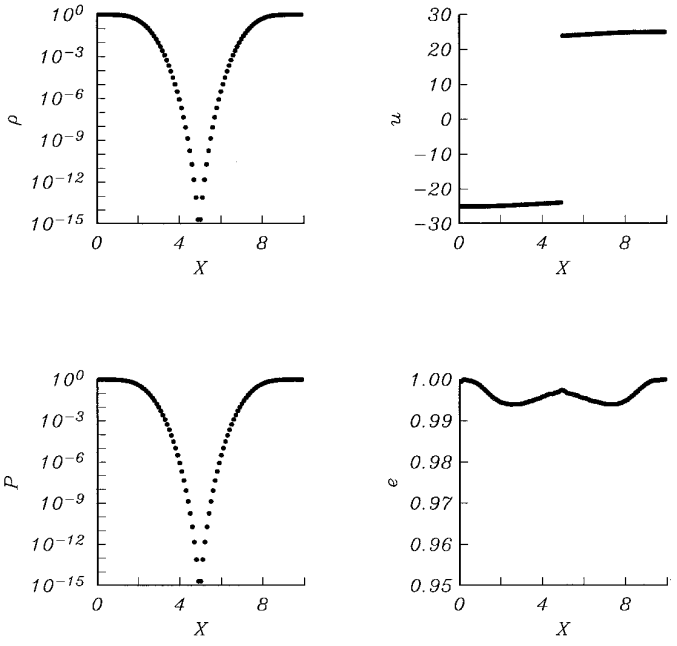

FIG. 7. Receding flow, $M_L = -M_R = -25$ by AUSM$^+$, first-order solution.

Since $u^+ \geq 0$, $u^- \leq 0$, $\lambda > 0$, and $\rho_j^0 > 0$ $\forall j$ (54) immediately gives

$$\rho_j^n \geq 0, \quad n > 0 \quad \forall j, \tag{55}$$

under condition (51). Hence, the positivity of the density is preserved. ▌

And (51) is called the *positivity condition.* For the linear case, this condition also coincides with the TVD condition of Harten [17].

Remark. Similar conditions for second-order accurate schemes can be derived as well, but allowing smaller λ, as shown in [3].

In Fig. 7 we demonstrate the effectiveness of the positivity-preserving property for the case of a receding flow in which two flows are moving away from each other at $M = 25$. The AUSM$^+$ scheme reachs a machine-zero density (vacuum condition) without difficulty, while the Roe and Osher–Solomon schemes will immediately encounter negative density. We note that the initial condition considered in this case is well beyond the Osher–Solomon scheme's limit for preserving positive sonic speed at the contact discontinuity, namely $-(\gamma - 1)(u_{j+1} - u_j)/2 + a_j + a_{j+1} \geq 0$.

Next we investigate the limiting form of the flux valid for the boundary layer flow where the transverse Mach number is small, $m_{1/2} \ll 1$. Assuming $m_{1/2} > 0$, the y–momentum flux (cf. (42)) becomes, by retaining only leading terms,

$$\begin{aligned} g_{j+1/2} = {} & \overline{M}\,\overline{\mathbf{\Phi}}(1 - \tfrac{1}{2}\Delta_{j+1/2}M) - \tfrac{1}{2}\overline{M}(1 - \tfrac{1}{2}\Delta_{j+1/2}M)\,\Delta\mathbf{\Phi} \\ & + \overline{\mathbf{P}}(1 - \tfrac{3}{2}\Delta_{j+1/2}pM + \cdots), \end{aligned} \tag{56}$$

where the overbar denotes the simple algebraic average, e.g., $\overline{M} = \frac{1}{2}(M_j + M_{j+1})$. Since the leading terms coincide with the central-difference approximation, the nominally first-order upwind formula now tends to be second-order accurate as $M \to 0$.

4.2. *Adding AUSM$^+$ to Existing Codes*

It is only a simple matter to add the AUSM$^+$ to a code having the Van Leer–Hänel splitting [11, 15]. First, all one needs is to use the numerical speed of sound $a_{j+1/2}$, instead of individual a_j and a_{j+1}, for defining M_j and M_{j+1}. Then define $m_{j+1/2}^{\pm}$ and substitute them for the "$\pm$" Mach numbers, i.e., $\mathscr{M}_j^+$ and $\mathscr{M}_{j+1}^-$, used in the Van Leer–Hänel splitting.

It is also an easy task to implement the AUSM$^+$ to a basic central-differencing code, only requiring the key interface quantities $(m_{j+1/2}, p_{j+1/2})$ once $a_{j+1/2}$ has been defined. As already derived in (46), we have

$$2p_{j+1/2} = (p_j + p_{j+1}) - \delta p_{j+1/2}. \tag{46}$$

We get, similarly,

$$\begin{aligned} 2m_{j+1/2} &= (M_j + M_{j+1}) - (\mathscr{M}_{j+1}^+ - \mathscr{M}_{j+1}^-) + (\mathscr{M}_j^+ - \mathscr{M}_j^-), \\ &= (M_j + M_{j+1}) - \delta m_{j+1/2}, \end{aligned} \tag{57}$$

where

$$|\mathscr{M}|(M) = \mathscr{M}^+(M) - \mathscr{M}^-(M), \tag{58a}$$

$$\delta m_{j+1/2} = |\mathscr{M}|(M_{j+1}) - |\mathscr{M}|(M_j), \tag{58b}$$

and

$$|\mathscr{M}|(M) = \begin{cases} |M|, & \text{if } |M| \geq 1, \\ \frac{1}{2}(M^2 + 1) + 2\beta(M^2 - 1)^2, & \text{otherwise.} \end{cases} \tag{59}$$

Since $|\mathscr{M}| > 0$ $\forall M$, the absolute sign applied to $\mathscr{M}$ makes sense. On the other hand, $\Delta\mathscr{P}$ in (48) can be either positive or negative, depending on the sign of M.

Once the quantities $(\delta p_{j+1/2}, \delta m_{j+1/2})$ have been defined, the dissipative terms derived from the AUSM$^+$ are ready

to be added. Rewriting the AUSM$^+$ flux in terms of the central-difference (CD) formula yields

$$\mathbf{f}_{j+1/2}^{AUSM^+} = \mathbf{f}_{j+1/2}^{CD} - \frac{a_{j+1/2}}{2}\left[\left(\frac{1}{2}\,\delta m_{j+1/2} - |m_{j+1/2}|\right)\mathbf{\Phi}_j + \left(\frac{1}{2}\,\delta m_{j+1/2} + |m_{j+1/2}|\right)\mathbf{\Phi}_{j+1}\right] - \frac{1}{2}\begin{pmatrix} 0 \\ \delta p_{j+1/2} \\ 0 \end{pmatrix}. \tag{60}$$

This is all there is to it.

5. BOUNDARY CONDITION

Two approaches are commonly used for implementing boundary conditions: (1) extend the computation domain with additional "ghost" cells and then assume some kind of reflection (mirror-image) conditions and (2) apply data extrapolated from the interior points, usually via characteristic relations, at the boundary. Since the convective fluxes vanish at the stationary and nonporous boundaries, the second approach amounts to only requiring pressure there; see (61) below. Moreover, it avoids the use of ghost cells. Hence, we prefer this approach.

We assert, as evident from the following example, that there is a tight relation between the interior scheme and the selection of an appropriate boundary conditions. In other words, the compatibility between a numerical flux scheme and boundary scheme must be observed. One example is the shock reflection at the end (closed in this case) of a shock tube. For example, a regular extrapolated condition for steady flow,

$$p_w := p_i, \qquad \bullet\ i \quad \bullet\ w$$

was applied in conjunction with the AUSM$^+$ to the standard Sod problem. We see in Fig. 8a the short-wave oscillations (not odd–even decoupling) bounded between the end and the shock, also reported in Ref. [26]. This phenomenon happened only in the higher order solution and the first-order solution appeared to have sufficient dissipation to suppress the high-frequency mode, since it appeared only after the boundary condition had taken effect for this problem as the shock was reflected from the end. (The same phenomenon was also evident at the other end, where the rarefaction wave was reflected.) Clearly this suggests that the root of the problem lies in the treatment of the numerical boundary condition.

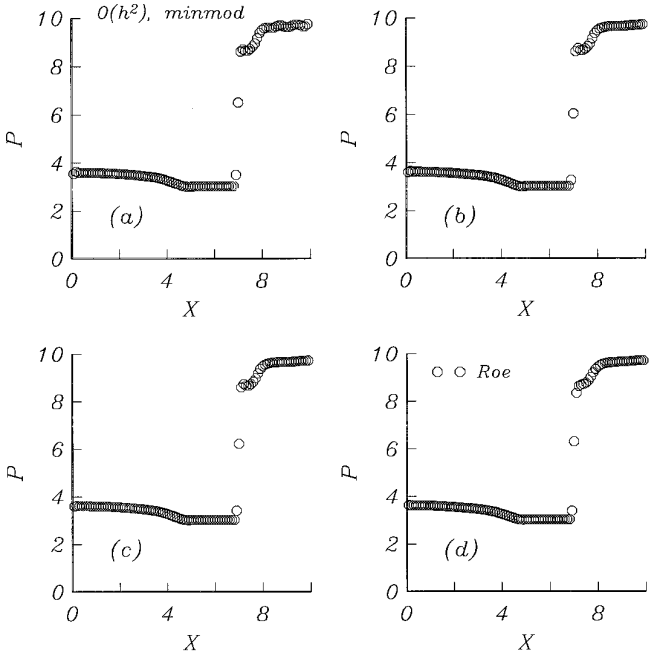

FIG. 8. Effect of boundary condition on the shock tube solution: (a) spatial extrapolation, $p_w = p_i$; (b) characteristic relation, (63); (c) characteristic relation, (64); and (d) Roe's splitting with (64).

After imposing the condition of zero-normal velocity component, the inviscid numerical flux is simply

$$\mathbf{f}_w = (0, p_w\vec{n}_w, 0), \quad \text{since } u_w = \vec{u}_w \bullet \vec{n}_w = 0. \tag{61}$$

Clearly p_w is the *key* for correcting the oscillations seen previously.

We again stress that it is desirable to have a boundary scheme compatible with the interior scheme. Since our interior scheme is basically constructed to be consistent with the concept of characteristics for nonlinear fields to relate p and u, we will begin by considering the characteristic equations:

$$\left(\frac{\partial u}{\partial t} \pm \frac{1}{\rho a}\frac{\partial p}{\partial t}\right) + (u \pm a)\left(\frac{\partial u}{\partial x} \pm \frac{1}{\rho a}\frac{\partial p}{\partial x}\right) = 0. \tag{62}$$

This set of equations has also been used in the papers by Moretti and co-workers (see, for instance, [27]). Considering the flow is subsonic near the boundary, we can connect the first interior and wall points (denoted by subscripts "i" and "w," respectively) via the $u \pm a$ waves. An approximate discrete equation for $u_w = 0\ \forall t \geq 0$ is

$$p_w^{n+1} = p_w^n(1 - 2\lambda a_i^n) + 2\lambda p_i^n(a_i^n \pm \gamma u_i^n), \quad \lambda = \Delta t/\Delta x. \tag{63}$$

Alternatively, an approximate form can be found by direct

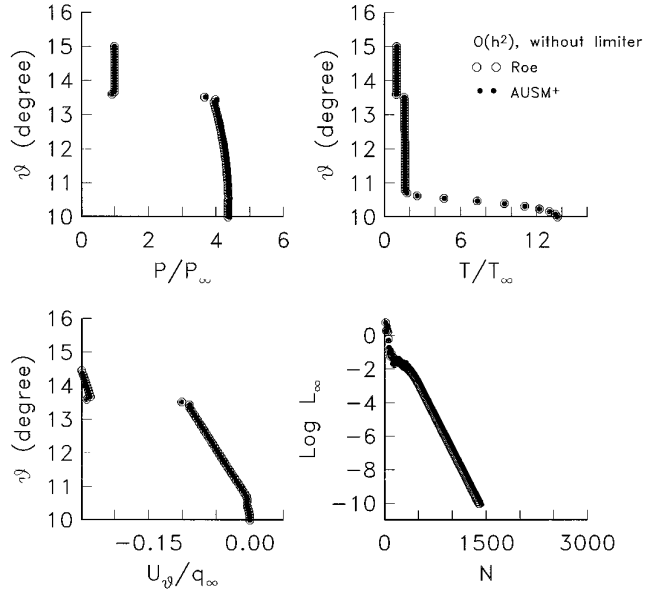

FIG. 9. Hypersonic conic flow; comparison of the AUSM$^+$ and Roe solutions.

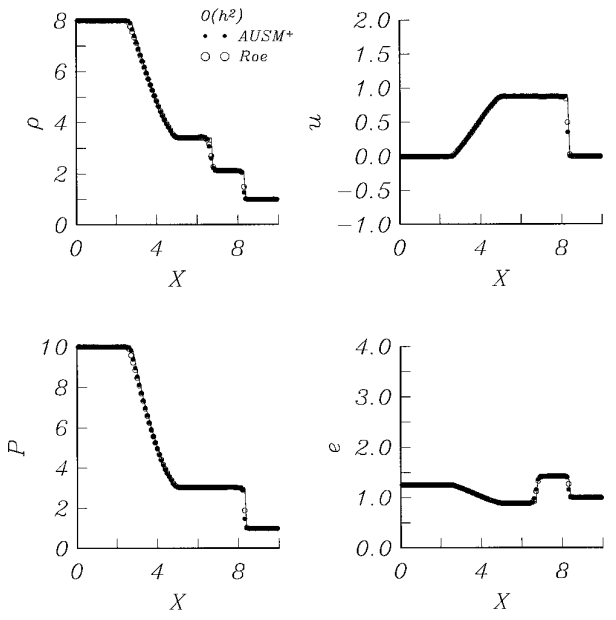

FIG. 10. Sod problem; comparison of the AUSM$^+$ and Roe solutions.

linearization and integration of the characteristic equation of (14):

$$p_w^{n+1} = p_i^n \pm u_i^n \rho_i^n a_i^n. \tag{64}$$

Both formulas are found to dramatically remove the short-wave oscillation, as demonstrated in Fig. 8, and the results are comparable with that of Roe's splitting using the same set of boundary conditions. In all the remaining calculations, the simpler formula (64) was used and oscillation-free results will become evident in Section 7.

6. HIGHER-ORDER EXTENSION

The MUSCL [19] strategy for preserving monotonicity is adopted here, via the use of a nonlinear limiter sensing the ratio of neighboring first-differences of appropriate variables. We choose to extrapolate the primitive variables **W**, according to the formulas

$$\begin{aligned} \mathbf{W}_L &:= \mathbf{W}_j + \frac{1}{2}\psi(r_j)(\mathbf{W}_j - \mathbf{W}_{j-1}), \\ \mathbf{W}_R &:= \mathbf{W}_{j+1} - \frac{1}{2}\psi\left(\frac{1}{r_{j+1}}\right)(\mathbf{W}_{j+2} - \mathbf{W}_{j+1}), \end{aligned} \tag{65}$$

where the subscripts "L" and "R" represent the states that take the place of "j" and "$j + 1$" in the formulas derived in Section 3 for the first-order scheme. To take grid nonuniformity into account, grid-size weighting can also be formulated into (65) if desired (see, for example, [28]). The function ψ is a limiter whose argument is defined as

$$r_j = \frac{\Delta_{j+1/2} w_i}{\Delta_{j-1/2} w_i}, \quad \mathbf{W} = (w_1, w_2, w_3)^{\mathrm{T}}. \tag{66}$$

We stress that the set of primitive variables $\mathbf{W} = (\rho, u,$

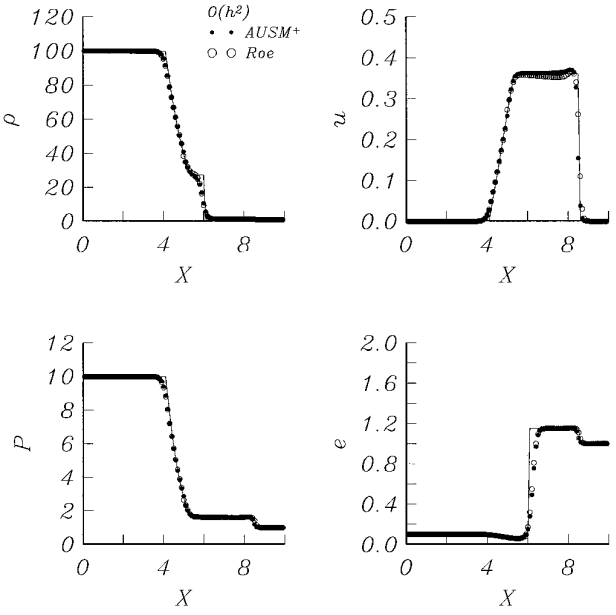

FIG. 11. Problem C; comparison of the AUSM$^+$ and Roe solutions.

$h_t)^T$ is employed and the minmod function is normally chosen for its robustness in our calculations. Other forms for the limiter function have been proposed and it is generally known that the accuracy of solution around discontinuities (shock or contact) is influenced more or less by the choice of the limiter. The dependence of the solution on the choice of the variables chosen for extrapolation in (65) also occurs. However, discussion of these aspects is beyond the scope of the present paper, but it can be found in the literature.

A majority of the results included in this paper are "second-order" accurate, unless it is stated explicitly when the first-order solutions are presented.

7. RESULTS AND DISCUSSION

In this section we demonstrate the capability of the proposed numerical flux by confirming the mathematical consequences established in previous sections for various relevant problems. The problems are listed below and will be discussed accordingly:

1. hypersonic conical boundary layer,
2. 1D shock tube problems,
3. 2D channel flow,
4. blunt body flow,
5. odd–even grid perturbation problem,
6. shock diffraction around a corner.

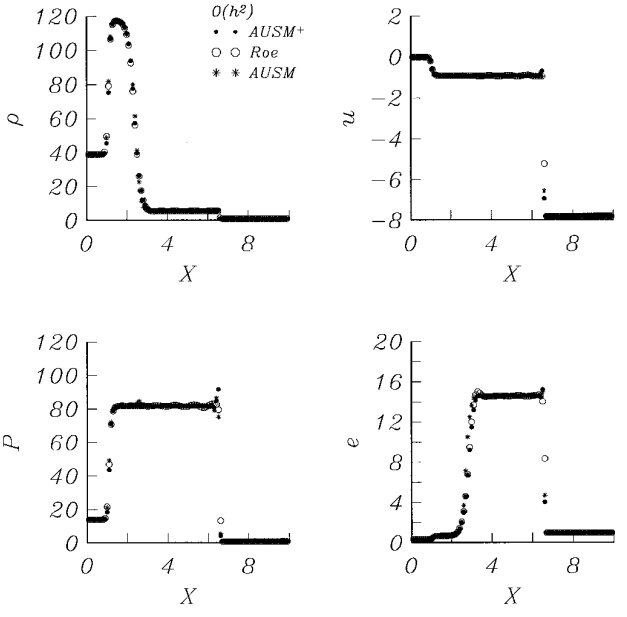

FIG. 12. Problem E; comparison of the AUSM, AUSM$^+$, and Roe solutions.

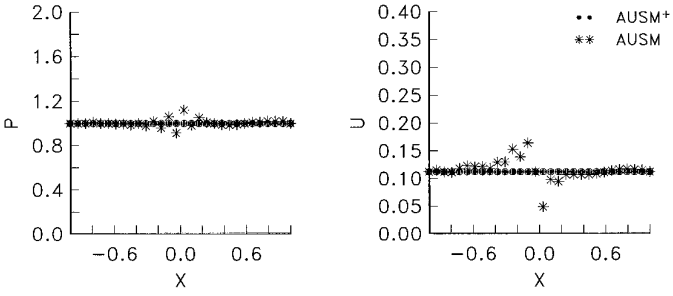

FIG. 13. Slowly moving contact; comparison of the first-order AUSM (*) and AUSM$^+$ (●) solutions.

For validation purposes, analytical solutions will be used as they are available. Otherwise, the solution will be compared with that obtained by using Van Leer's and Roe's splittings as they have been established as an accurate and very popular upwind scheme in use today. In some noted cases, we also include the AUSM solution in order to show the improvement of the present AUSM$^+$ splitting.

Most of this section will be devoted to establishing accuracy issues for all the above-listed problems, and it will be followed by study of the convergence history.

The first problem deals with the capability of accurately resolving a shock and a thin viscous layer. In problem 2, we are concerned with the accuracy in calculating unsteady flows. In problems 3 and 4, we consider 2D steady inviscid flows. Finally, 2D unsteady solutions are discussed in problems 5 and 6.

A two-step Runge–Kutta type explicit scheme [28] was used in the time-discretization for all of the above problems. Standard direction-by-direction approach to define numerical fluxes in multidimensions was employed and the higher order formula used in each respective direction.

7.1. *Accuracy*

The conical flow at $M_\infty = 7.95$ over a cone of 10° half angle was calculated using 64 cells. The profiles of pressure, temperature, and transverse velocity component are shown in Fig. 9 for the second-order results. The Roe and AUSM$^+$ splittings (denoted by ● and ○) give nearly identical results; interestingly the convergence rates also show remarkable resemblance. Note that there was no need to invoke a limiter function (i.e., setting $\psi = 1$ in (65)) for this calculation for both splittings; it is generally desirable to limit the use of limiters insofar as numerical stability is allowed, especially when physically true extrema are present (the tangential velocity component U_θ in this case).

Next we consider the shock-tube problems; calculations were done using 100 cells (unless stated otherwise) and CFL = 0.8. For the standard Sod problem, Fig. 10 clearly demonstrates the comparable accuracy of the present and the Roe solutions (denoted by ● and ○, respectively).

We now add two more difficult problems studied by Yee [20]; they correspond nearly to cases denoted as C and E in [20] in terms of density and pressure ratios and initial Mach number but without chemical effects. The initial conditions are:

$$\text{Case C: } (\rho, p, M)_L = (1, 1, 0), (\rho, p, M)_R = (\tfrac{1}{100}, \tfrac{1}{10}, 0), \quad (67a)$$

$$\text{Case E: } (\rho, p, M)_L = (1, 1, 0), (\rho, p, M)_R = (\tfrac{1}{39}, \tfrac{1}{14}, -7.8). \quad (67b)$$

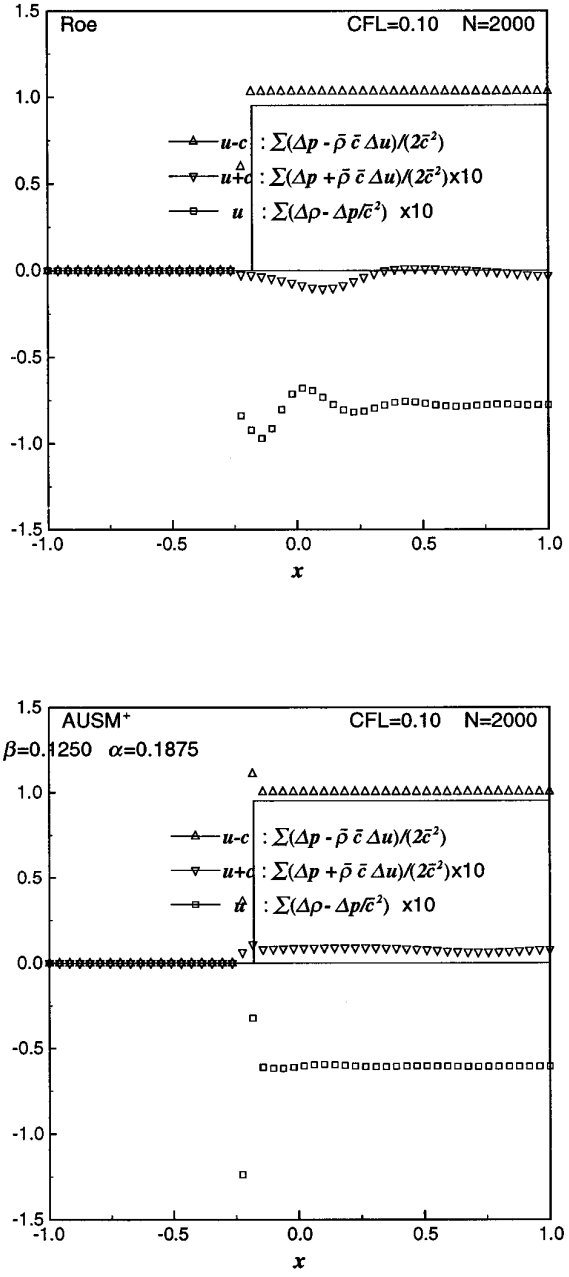

FIG. 14. Slowly moving shock; comparison of the first-order Roe (top) and AUSM$^+$ (bottom) solutions.

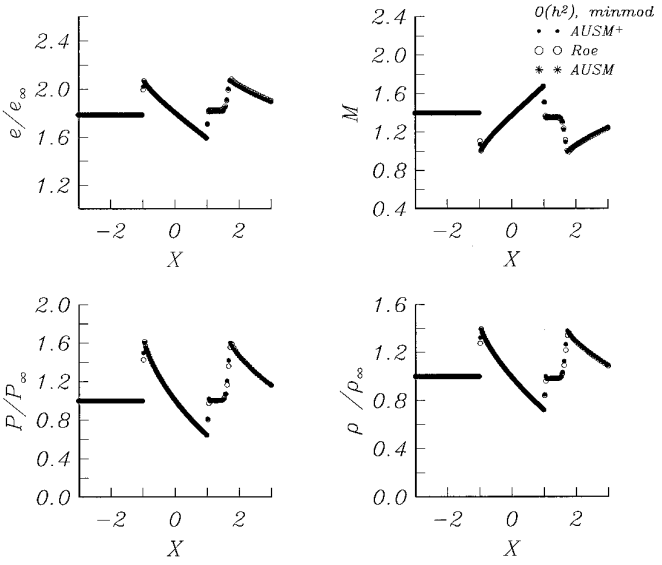

FIG. 15. Four percent bump problem; comparison solutions on the bump by the AUSM$^+$ (●●), AUSM (**), and Roe (○○) splittings.

The former involves a much stronger contact discontinuity than the Sod problem; the latter has a shock moving slowly against a high pressure region, with characteristics similar to those studied by Roberts [21] and with an additional large density jump. Figure 11 begins to show the differences between the results obtained using the AUSM$^+$ and Roe splittings. Immediately behind the shock, the AUSM$^+$ (denoted by ●) appears to give better agreement with the exact solution, it is more obvious in the plateau region of the velocity profile.

In the study of Roberts [21] and Lin [22], wave-like oscillations were observed in the Roe solution. This error

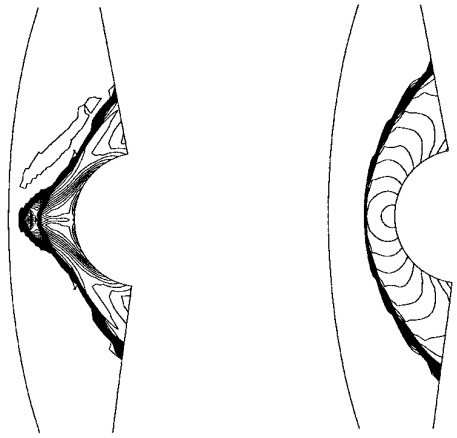

FIG. 16. Supersonic blunt body problem; Mach contours by the Roe method (left) and AUSM$^+$ (right).

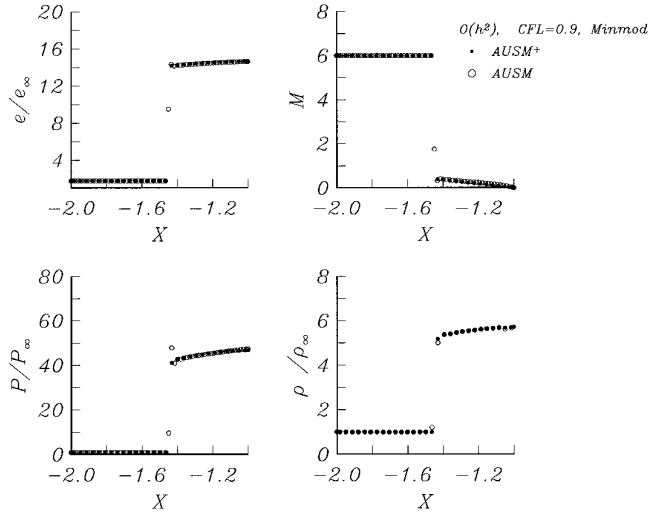

FIG. 17. Supersonic blunt body problem; comparison of the AUSM+ and AUSM solutions.

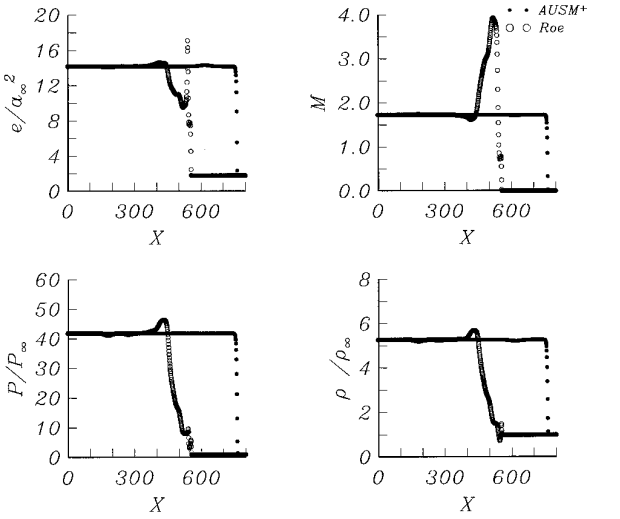

FIG. 19. Odd–even grid perturbation problem; profiles along the centerline by the AUSM+ (●●) and Roe (○○) splittings. Note that the Roe solution was terminated earlier.

also appears for this problem in Fig. 12 for the Roe solution (given by ○). Both AUSM+ and AUSM results are seen to be free from this behavior, but AUSM (denoted by *) gives rise to a glitch in the pressure due to a large gradient at the contact discontinuity. It is noted that the AUSM+ results have a higher overshoot value, immediately behind the shock, than the other two results; however, we deem this point less significant (although not desirable) than the ones mentioned above. The pressure glitch by the AUSM scheme is further confirmed by investigating an isolated slowly moving contact discontinuity in the first-order accurate solution; the results by AUSM and AUSM+ are displayed in Fig. 13, revealing a dramatic difference between them. The AUSM calculation did not seem to suggest instability in the sense of a disturbance amplifying without bound, but rather resulting in a corrupted solution in all variables. On the other hand, the AUSM+ solution behaves as it should.

To further illustrate the dispersive error introduced by numerical schemes in a slowly moving flow, we show in Fig. 14 the results for a shock slowly (50 time steps per cell) moving to the left. The results are presented in terms of a discrete representation of integral of the Riemann variables, i.e., $\int dp \pm \rho a du$ and $\int dp - a^2 d\rho$. The Roe solution clearly shows the wave-like error trailing behind the shock for the two downstream-running characteristics; the AUSM+ solution maintains nearly constant values, except with a jump at the shock, as it should be.

We turn now to 2D problems. The first case in this category is the standard 4% bump in a channel with $M_\infty = 1.4$. The results were obtained using the AUSM+, AUSM, and Roe splittings with minmod limiter, and CFL = 0.9 on a 132×68 grid. The profiles on the bump wall in Fig. 15 show that three solutions agree well and all give sharp representation of three shocks, two respectively located at the leading and trailing edge of the bump and

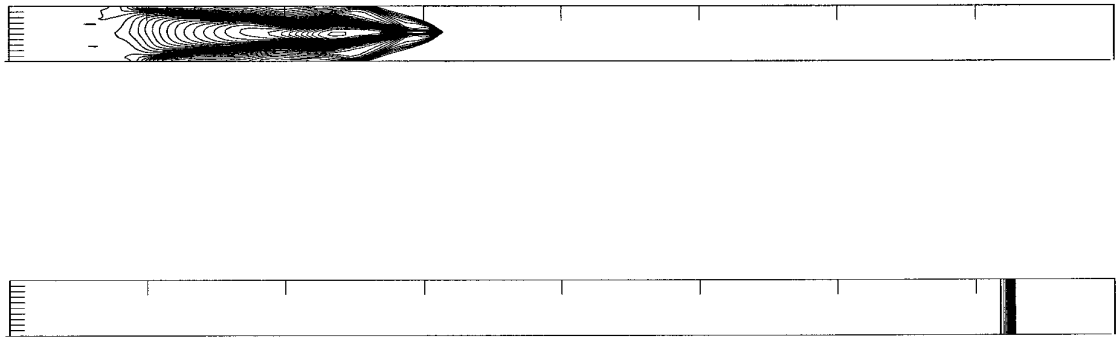

FIG. 18. Odd–even grid perturbation problem; Mach contours by the Roe method (top) and AUSM+ (bottom).

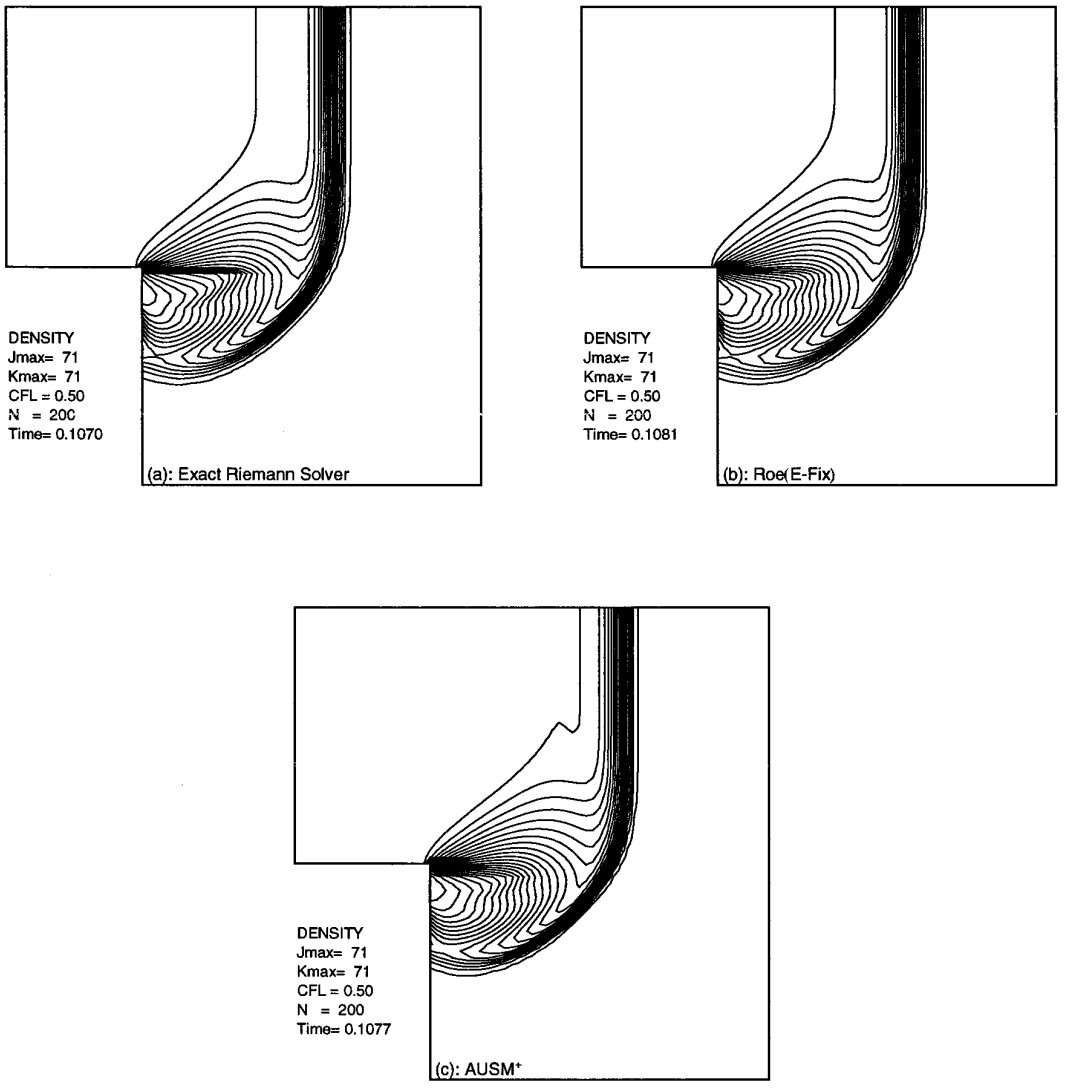

FIG. 20. Supersonic corner flow problem; density contours of first-order solution: (a) Gudonov method; (b) Roe method; and (c) AUSM$^+$.

one located further downstream and produced by the reflection of the leading-edge shock from the other wall.

Let us now consider a supersonic $M_\infty = 6.0$ flow over a circular cylinder. This seemingly benign problem in fact turns out to be rather daunting for some prominent schemes such as the Osher and Roe splittings [6, 22, 23]. The so-called ''carbuncle'' phenomenon produced by Roe's method is exhibited in Fig. 16, in comparison with that by the AUSM$^+$. Figure 17 displays the solutions by the AUSM and AUSM$^+$, showing a crisp shock resolution at the centerline. In particular, the AUSM$^+$ (denoted by ●) exhibits the evidence of improvement over the AUSM (denoted by ○), by eliminating the postshock overshoot, and with nearly no numerical shock point.

Next, we study another interesting and benign problem, first reported by Quirk [5]. A plane shock is moving into a quiescent region in a long constant-area channel. The computation grid is perturbed at the centerline by a very small magnitude, $\pm 10^{-6}$ in our case, alternately at odd and even points. The Roe solution, in Fig. 18 (top), quickly develops an odd–even decoupling behavior, eventually leading to a catastrophic solution. The present method, on the other hand, still preserves the plane shock even after a long time, as shown in Fig. 18 (bottom). The variable profiles along the centerline, corresponding to the contours, are displayed in Fig. 19 for comparison—the AUSM$^+$ gives a monotone and well-behaved solution.

The last problem is the diffraction of a supersonic shock moving over a 90° bend. Quirk [5] has painstakingly shown the complexity of the flow using grid refinement to resolve the fine details. He pointed out that there was some numerical difficulty encountered in the use of the Roe splitting.

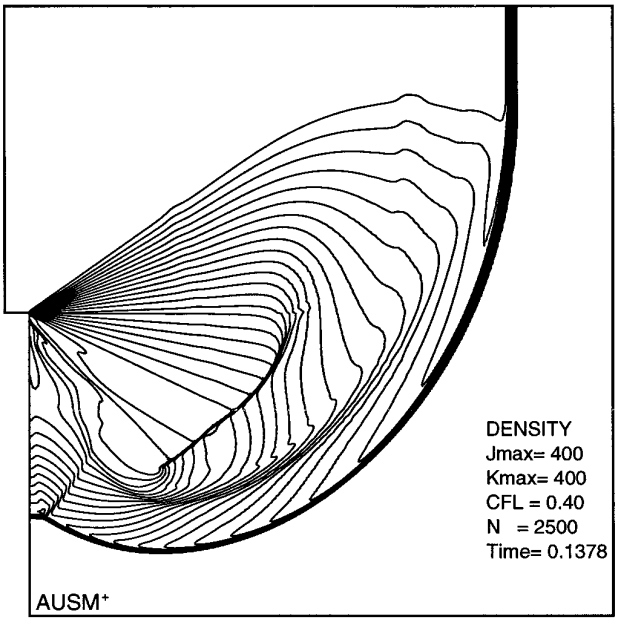

FIG. 21. Supersonic corner flow problem; density contours of second-order (with minmod limiter) AUSM$^+$ solution on 400 × 400 grid.

Thus it would be an interesting problem to test whether the present AUSM$^+$ would have any difficulty. First we show in Fig. 20 the density contours of first-order AUSM$^+$, Roe, and Godunov solutions on a 71 × 71 grid, which is extremely coarse to be able to reveal any intricate details. Nevertheless, it confirms the findings of Woodward and Collela [24] and Quirk [5] that the Godunov scheme can yield discontinuous expansion fans as seen in Fig. 20a—this, apparently violating the entropy condition, clearly causes concern. Figures 20b and 20c show that both the Roe splittings (with entropy fix) and AUSM$^+$, respectively, are able to break the numerical expansion shock. A fine grid (400 × 400) calculation was then performed using the minmod limiter and CFL = 0.4 (higher value, while still stable, gave oscillatory contours near the internal shock) and the result is depicted in Fig. 21. The intricacy associated with this flow is astonishingly rich, although what is contained at this grid level is still not nearly comparable to that captured by Quirk [5], who used a sophisticated adaptive grid strategy.

7.2. *Convergence History of Residual*

The convergence history for the supersonic 4%-bump problem is displayed in Fig. 22 in terms of L_2 norm, exhibiting that the Roe solution stalls after having dropped about five orders, while the AUSM$^+$ and AUSM residuals continue to decrease to machine accuracy, following roughly the same history.

Figure 23 compares the AUSM$^+$ convergence history

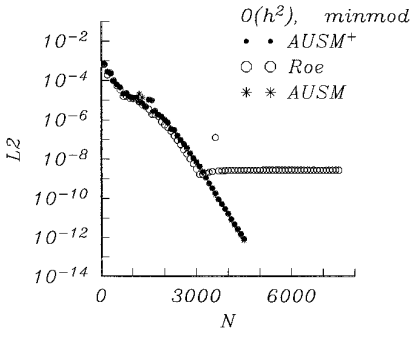

FIG. 22. Convergence history for the 4% bump problem; second-order solution.

for the blunt body problem, showing the effects of order of spatial accuracy, grid size, and CFL number. It is surprising to see that the second-order method in fact converges faster than the first-order method, even with the shock. On the other hand, it also reaffirms the benefit of achieving faster convergence rate by using larger CFL number and the adverse effect of slowing down convergence by running on a fine grid, as consistent with other published results.

8. CONCLUDING REMARKS

In this paper we presented the construction and analysis of a new numerical flux scheme—AUSM$^+$. We investigated the associated mathematical properties and proved the positivity-preserving property with a CFL-like condition. We proposed an enhanced set of Mach number and pressure polynomials, contributing to improvement in accuracy. Furthermore, a properly defined numerical speed of sound for the interface Mach number was shown to give exact resolution for an 1D steady shock and significantly improved shock resolution in 2D cases. The reliability of the new scheme was evident as well in calculating some unsteady problems that have failed prominent flux schemes. We also stress that in addition to the demonstrated accuracy and reliability, the AUSM$^+$ requires com-

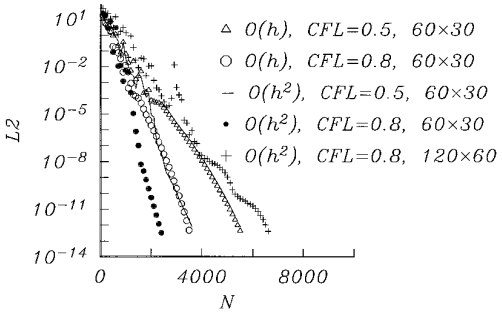

FIG. 23. Convergence history for the supersonic blunt body problem.

putational effort only linearly proportional to the number of equations considered. Furthermore, the scheme is amenable for easy extension to other system of conservation laws.

ACKNOWLEDGMENTS

It has been a very rewarding experience for the author working with Dr. Yasuhiro Wada who spent a year (1993–1994) at ICOMP, NASA Lewis Research Center, on leave from NAL of Japan. He kindly provided his code for calculating the shock diffraction around a 90° corner. Sadly he passed away untimely in March 1995. The author thanks the anonymous referees for making valuable suggestions which led to improvements of the paper.

REFERENCES

1. M.-S. Liou and C. J. Steffen Jr., A new flux splitting scheme, *J. Comput. Phys.* **107,** 23 (1993).
2. M.-S. Liou, "On a New Class of Flux Splitting," in Lecture Notes in Physics, Vol 414 (Springer-Verlag, New York/Berlin, 1993), p. 115.
3. M.-S. Liou, NASA TM 106524, March 1994 (unpublished).
4. P. L. Roe, "A Survey of Upwind Differencing Techniques," in Lecture Notes in Physics, Vol. 323 (Springer-Verlag, New York/Berlin, 1989), p. 69.
5. J. J. Quirk, ICASE Report 92-64, 1992 (unpublished).
6. Y. Wada and M.-S. Liou, An accurate and robust flux splitting scheme for shock and contact discontinuities, *SIAM J. on Scientific Computing,* to appear in 1977; also AIAA 94-0083 (unpublished).
7. F. Coquel and M.-S. Liou, "Stable and Low Diffusive Hybrid Upwind splitting Methods," in *Proceedings of the First European Computational Fluid Dynamics Conference, 1992,* Vol. 1, p. 9.
8. F. Conquel and M.-S. Liou, "Field by Field Hybrid Upwind Splitting Methods," in *11th AIAA CFD Conference;* AIAA Paper 93-3302-CP, 1993.
9. F. Coquel and M.-S. Liou, NASA TM 95-2, 1995 (unpublished).
10. J. L. Steger and R. F. Warming, Flux vector splitting of the inviscid gasdynamics equations with application to finite difference methods, *J. Comput. Phys.* **40,** 263 (1981).
11. B. van Leer, "Flux-Vector Splitting for the Euler Equations," in Lecture Notes in Physics, Vol. 170 (Springer-Verlag, New York/Berlin, 1982), p. 507.
12. J. A. Owczarek, *Fundamentals of Gas Dynamics* (International Textbook, Scranton, PA, 1964).
13. P. L. Roe, Approximate Riemann solvers, parameter vectors and difference schemes, *J. Comput. Phys.* **43,** 357 (1981).
14. S. Osher and F. Solomon, Upwind difference schemes for hyperbolic systems of conservation laws, *Math. Comp.* **38,** 339 (1982).
15. D. Hänel, R. Schwane, and G. Seider, "On the Accuracy of Upwind Schemes for the Solution of the Navier-Stokes Equations," in *8th AIAA CFD Conference;* AIAA paper 87-1105-CP, 1987.
16. B. Larrouturou, How to preserve the mass fractions positivity when computing compressible multi-component flows, *J. Comput. Phys.* **95,** 59 (1991).
17. A. Harten, A high resolution scheme for the computation of weak solutions of hyperbolic conservation laws, *J. Comput. Phys.* **49,** 357 (1983).
18. B. van Leer, J. L. Thomas, P. L. Roe, and R. W. Newsome, in *8th AIAA CFD Conference,* AIAA Paper 87-1104CP, 1987.
19. B. van Leer, Towards the ultimate conservation difference scheme. V. A second-order sequel to Godunov's method, *J. Comput. Phys.* **32,** 101 (1979).
20. H. C. Yee, NASA TM 89464, 1987 (unpublished).
21. T. W. Roberts, The behavior of flux difference splitting schemes near slowly moving shock waves, *J. Comput. Phys.* **90,** 141 (1990).
22. H.-C. Lin, "Dissipation Additions to Flux-Difference Splitting," in *10th AIAA Computational Fluid Dynamics Conference,* AIAA Paper 91-1544, 1991.
23. K. M. Peery and S. T. Imlay, "Blunt-Body Flow Simulations," in *AIAA/SAE/ASME/ASEE 24th Joint Propulsion Conference,* AIAA Paper 88-2904, 1988.
24. P. R. Woodward and P. Collela, The numerical simulation of two-dimensional fluid flow with strong shocks, *J. Comput. Phys.* **54,** 115 (1984).
25. A. Jameson, "Artificial Diffusion, Upwind Biaing, Limiters and their Effect on Accuracy and Multigrid Convergence in Transonic and Hypersonic Flows," in *11th AIAA CFD Conference,* AIAA Paper 93-3359, 1993.
26. L. Bergamini and P. Cinnella, Using the Liou–Steffen algorithm for the Euler and Navier–Stokes equations, *AIAA J.* **32,** 657 (1994).
27. G. Moretti and M. Pandolfi, Critical study of calculations of subsonic flows in ducts, *AIAA J.* **19,** 449 (1981).
28. M.-S. Liou and A. T. Hsu, "A Time Accurate Finite Volume High Resolution Scheme for Three Dimensional Navier-Stokes Equations," in *9th AIAA CFD Conference,* AIAA Paper 89-1994-CP, 1989.
29. J. R. Edwards, An implicit multigrid algorithm for computing hypersonic, chemically reacting viscous flows, *J. Comput. Phys.* **123,** 84 (1996).
30. I. Men'shov and Y. Nakamura, "An Implicit Advection Upwind Splitting Scheme for Hypersonic Air Flows in Thermochemical Nonequilibrium," in *Proceedings, 6th International Symposium on Computational Fluid Dynamics, Vol. II, 1995,* p. 815.